Explicit Numerical Solution of the Three-Dimensional Incompressible Turbulent Boundary-Layer Equations

J. L. EAST JR.*
Naval Weapons Laboratory, Dahlgren, Va.
AND
F. J. PIERCE†
Virginia Polytechnic Institute and State University, Blacksburg, Va.

An explicit finite-difference technique has been developed and applied to solve the governing partial differential equations for the three-dimensional incompressible turbulent boundary layer. The method uses a mixing-length concept suggested by Prandtl for representing the turbulent shear stress tensor. The only empirical input is a mathematical model for the mixing length taken after Maise and McDonald which incorporates the van Driest damping factor in the near-wall flow region. The predicted boundary-layer parameters and the velocity profiles agree well with the experimental data for two geometries considered, both of which contained a plane of symmetry with large transverse gradients in flow properties to provide a severe test of the method of solution and to a lesser extent the shear model. The analysis does not indicate a collateral near-wall layer as suggested by several experiments.

Nomenclature

C_f = skin-friction coefficient
I, J, K = lattice or grid indices
l = mixing length
L = nondimensionalized mixing length
T = defined in Eq. (6)
u, v, w = time-average x, y, z velocity components in the boundary layer
ue, we = time-average x, z velocity components at the boundary-layer edge
u_s, w_s = time average velocity components in the boundary layer in the freestream and transverse directions
$u_s e, w_s e$ = time average velocity components at the boundary-layer edge in freestream and transverse directions
$u'v'; w'v'$ = Reynolds' turbulent stresses
u^* = shear velocity $(\tau_w/\rho)^{1/2}$
u_0^* = reference shear velocity
U, V, W = nondimensionalized time-average x,y,z velocity components in the boundary-layer
UE, WE = nondimensionalized time-average x,z velocity components at the boundary-layer edge
x, y, z = Cartesian space coordinates
X, Y, Z = nondimensionalized space coordinates
y^+ = dimensionless wall distance u^*y/ν
κ = von Kármán constant 0.41
δ = boundary-layer thickness
ν = kinematic viscosity
ρ = mass density
$\Delta X, \Delta Y, \Delta Z$ = space increments

Subscripts

x, y, z = derivatives
$+, -$ = forward or backward increment

Introduction

THE development of modern high-speed digital computers in recent years has lead to a variety of solution schemes for the two-dimensional turbulent boundary-layer equations in their partial differential form as summarized by the recent proceedings from Stanford[1] and NASA-Langley.[2] The exact numerical integration techniques involve the replacement of the partial differential equations by suitable difference equations whose truncation errors can be made small by a proper choice of the solution grid spacing. Implicit marching integration is perhaps the most frequently used method. This technique was introduced by Crank and Nicholson[3] for the transient heat conduction equation and has been used successfully in fluid dynamics. The procedure consists of laying a finite-difference grid over the flowfield and calculating the values of fluid properties at the grid nodes along a line moral to the main flow direction by means of algebraic equations. After values along this line are determined, the solution is repeated one step further downstream.

Solution schemes for the three-dimensional turbulent boundare-layer case are by contrast sparse. Bradshaw[4] and Nash[5,6] have used the turbulence energy equation to relate the turbulent stresses to the mean flowfield properties. This model excludes any wholly viscous stresses and hence does not allow near-wall calculations within the laminar sublayer, with the usual no-slip boundary condition replaced by some matching scheme to some three-dimensional adaptation of the universal inner law. Thus details of the near-wall behavior of the flow are not directly available from such a model. Mellor[7] has solved the plane of symmetry problem using an eddy-viscosity model. Hunt, Bushnell, and Beckwith[8] have presented results based on a mixing length model for an infinite swept wing in compressible flow, but this latter case, while more complex in including compressibility effects simplifies the equations considerably by the exclusion of transverse gradients.

The present work has incorporated the marching integration concept in the development and evaluation of a solution technique for the full three-dimensional turbulent boundary-layer equations. A mixing length hypothesis replaces the turbulent shear stress tensor, but viscous stresses are also retained so as to predict full details of the near-wall flowfield. The mathematical representation for the mixing length variable was based on work by Maise and McDonald[9] and includes the van Driest[10] damping factor in the flow regions near the wall boundary.

An explicit set of finite-difference equations, patterned after the DuFort-Frankel scheme,[11] allowed larger marching steps to be taken in the solution than would have been possible with a simple two-point explicit scheme which is restricted in step size because of stability considerations. The excellent agreement with experimental data available for two three-dimensional flow geometries considered, both of which have large transverse gradients in flow properties to provide a severe test for the solution method and to a lesser extent the shear model, indicates

Received August 6, 1971; revision received March 22, 1972.
Index category: Boundary Layers and Convective Heat Transfer—Turbulent

* Research Engineer.
† Professor, Mechanical Engineering. Member AIAA.

the ability of the solution technique to mathematically predict three-dimensional turbulent boundary-layer flows.

Governing Equations and Boundary Conditions

Partial Differential Equations

The time average Navier-Stokes equations are written making the usual boundary-layer assumptions for steady flow over a nearly flat surface located on a y plane in a Cartesian coordinate system with

$$uu_x + vu_y + wu_z = ue(ue)_x + we(ue)_z + vu_{yy} + (-u'v')_y \quad (1)$$

$$uw_x + vw_y + ww_z = ue(we)_x + we(we)_z + vw_{yy} + (-w'v')_y \quad (2)$$

$$u_x + v_y + w_z = 0 \quad (3)$$

where the pressure gradient terms have been written in terms of the Euler equations of the boundary-layer edge. The fluid viscosity and density are considered as constant.

Turbulent Stress Terms

A model for the turbulent stress terms $u'v'$ and $w'v'$ and sufficient boundary conditions are required to solve Eqs. (1–3). From the generalized three-dimensional mixing length hypothesis given by Prandtl and presented by Goldstein[12] one may write

$$-u'v' = l^2T(v_x + u_y) \quad (4)$$

$$-w'v' = l^2T(v_x + w_y) \quad (5)$$

where

$$T^2 = 2(u_x)^2 + 2(v_y)^2 + 2(w_z)^2 + (w_y + v_z)^2 + (u_z + w_x)^2 + (v_x + u_y)^2 \quad (6)$$

and l is the mixing length parameter.

Equations (4–6) with boundary-layer order–of–magnitude considerations give the following expressions for the turbulent stress terms

$$-u'v' = l^2[(u_y)^2 + (w_y)^2]^{1/2}u_y \quad (7)$$

$$-w'v' = l^2[(u_y)^2 + (w_y)^2]^{1/2}w_y \quad (8)$$

so that Eqs. (1–3) become

$$uu_x + vu_y + wu_z = ue(ue)_x + we(ue)_z + (\{v + l^2[(u_y)^2 + (w_y)^2]^{1/2}\}u_y)_y \quad (9)$$

$$uw_x + vw_y + ww_z = ue(we)_x + we(we)_z + (\{v + l^2[(u_y)^2 + (w_y)^2]^{1/2}\}w_y)_y \quad (10)$$

$$u_x + v_y + w_z = 0 \quad (11)$$

which contain the known fluid properties, the three unknown velocity vector components and their derivatives, and the mixing length l, which is assumed to be isotropic.

In this analysis the mixing length was taken from the recent work by Pletcher,[13] who expressed the results of Maise and McDonald[9] as

$$l/\delta = \kappa[1.0 - \exp(-y^+/26)]\,(y/\delta), \quad y/\delta < 0.1 \quad (12)$$

$$l/\delta = \kappa[1.0 - \exp(-y^+/26)]\,(y/\delta) - 1.53506(y/\delta - 0.1)^2 + 2.75625(y/\delta - 0.1)^3 - 1.88425(y/\delta - 0.1)^4, \quad 0.1 \leqq y/\delta \leqq 0.6 \quad (13)$$

$$l/\delta = 0.089, \quad y/\delta > 0.6 \quad (14)$$

which includes the van Driest[10] damping factor for the near-wall flow. The universal mixing parameter κ is taken as the von Kármán constant equal to 0.41. The value of friction velocity u^*, required in determining y^+, is obtained by using the first derivative of the total velocity vector magnitude at the boundary wall since in the finite-difference solution the first few grid locations off the boundary wall are well within the viscous sublayer where Newton's law of friction is adequate. One reservation in extending these equations to yield a mixing length for the three-dimensional flowfield is that the wall shear stress in a three-dimensional boundary-layer flow is not necessarily directed along the freestream direction (Johnston[14]) as in two-dimensional flows. Evident need exists for more experimental turbulence data in three-dimensional flows so that a more critical evaluation can be made of the use of this mathematical model.

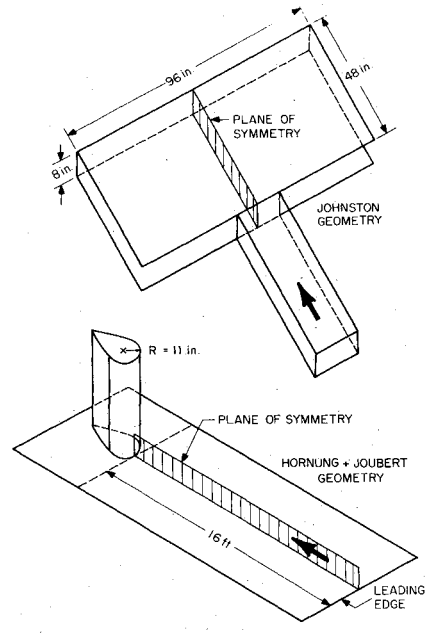

Fig. 1 Isometric view of experimental geometries.

Boundary Conditions

A solution to Eqs. (9–11) requires one set of conditions along a constant x plane, two sets of conditions in the y direction, and one set of conditions on a constant z plane. Computer results for the solution technique were compared to experiments where a three-dimensional turbulent boundary-layer was generated on the confining wall of an impinging flow as shown in Fig. 1; in one case the flow impinged on a flat wall and in another on a cylindrical shaped body protruding from the floor. In both circumstances the far upstream flow was essentially without three-dimensional effects so that a solution was started from the leading edge of a flat plate and a match made with the experimental data in the velocity profiles and boundary-layer parameters at an appropriate location where the three-dimensional effects were small, with the three-dimensional calculation scheme implemented thereafter.

No-slip applied as a boundary condition at the $y = 0$ plane. The second boundary condition in y was the specification of the boundary-layer edge condition as a freestream condition which followed from a potential solution for the appropriate freestream flow.

The boundary conditions on a constant z plane were obtained at the plane of symmetry. Thus a plane of symmetry solution be-

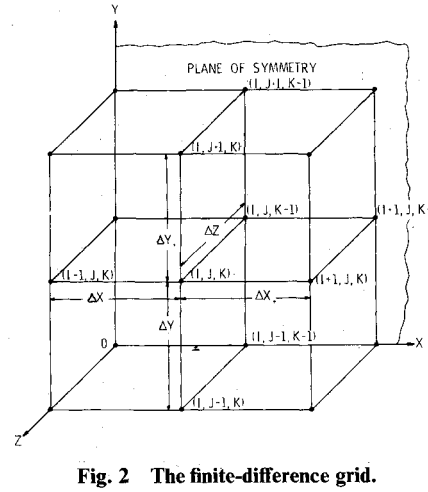

Fig. 2 The finite-difference grid.

came a necessary part of the full three-dimensional solution, with the former providing a boundary condition for the latter. The governing equations for the plane of symmetry are given below, where Eq. (16) follows by differentiating Eq. (10) with respect to z before the simplifying conditions on the plane of symmetry, $w = u_z = v_z = w_{zz} = w_x = w_y = 0$, were introduced.

$$uu_x + vu_y = ue(ue)_x + ([v + l^2u_y]u_y)_y \tag{15}$$

$$u(w_z)_x + v(w_z)_y + (w_z)^2 = ue(we_z)_x + (we_z)^2 + [(v + l^2u_y)(w_z)_y]_y \tag{16}$$

$$u_x + v_y + w_z = 0 \tag{17}$$

Normalized Equations

The velocity terms were made dimensionless by a representative shear velocity, u_o^*, and all lengths were normalized by v/u_o^*. In the normalized form the governing equations for the full three-dimensional flowfield are

$$UU_X + VU_Y + WU_Z = UE(UE)_X + WE(UE)_Z + (\{1 + L^2[(U_Y)^2 + (W_Y)^2]^{1/2}\}U_Y)_Y \tag{18}$$

$$UW_X + VW_Y + WW_Z = UE(WE)_X + WE(WE)_Z + (\{1 + L^2[(U_Y)^2 + (W_Y)^2]^{1/2}\}W_Y)_Y \tag{19}$$

$$U_X + V_Y + W_Z = 0 \tag{20}$$

and for the plane of symmetry are

$$UU_X + VU_Y = UE(UE)_X + [(1 + L^2U_Y)U_Y]_Y \tag{21}$$

$$U(W_Z)_X + V(W_Z)_Y + (W_Z)^2 = UE(WE_Z)_X + (WE_Z)^2 + [(1 + L^2U_Y)(W_Z)_Y]_Y \tag{22}$$

$$U_X + V_Y + W_Z + 0 \tag{23}$$

Finite-Difference Equations

A standard explicit finite-difference scheme was first used to represent the sets of partial differential equations. A stability criterion following the von Neumann condition as presented by O'Brien et al.[15] indicated a restrictively small marching step size and subsequently a time consuming calculating procedure subject to round-off error buildup. The direct scheme for writing the equations in an explicit stable form was taken from the method proposed by DuFort and Frankel.[11] The standard explicit equations were used to start the stable equations solution since the DuFort-Frankel formulation requires information at two previous streamwise locations. The three-dimensional grid shown in Fig. 2 is presented to help in interpreting the following equations.

A thorough discussion of the distinctions between the standard explicit method and the DuFort-Frankel type scheme is made by Pletcher[13] in his work on a similar solution technique for the two-dimensional case. Differences which occur in the three-dimensional formulation should be clear from the difference equations themselves.

The full three-dimensional equations written in the DuFort-Frankel scheme are

X-momentum:

$$U(I,J,K)\left(\frac{U(I+1,J,K) - U(I-1,J,K)}{(\Delta X_+ + \Delta X_-)}\right) + V(I,J,K)\left(\frac{U(I,J+1,K) - U(I,J-1,K)}{(\Delta Y_+ + \Delta Y_-)}\right) + W(I,J,K)\left(\frac{U(I,J,K) - U(I,J,K-1)}{\Delta Z}\right) = UE(I,K)\left(\frac{UE(I+1,K) - UE(I-1,K)}{(\Delta X_+ + \Delta X_-)}\right) + WE(I,K)\left(\frac{UE(I,K) - UE(I,K-1)}{\Delta Z}\right) + \frac{2}{(\Delta Y_+ + \Delta Y_-)}\left(\left\{1 + \left(\frac{L^2(J+1) + L^2(J)}{2}\right)\right.\right.$$
$$\cdot\left[\left(\frac{U(I,J+1,K) - (1/2)[U(I+1,J,K) + U(I-1,J,K)]}{\Delta Y_+}\right)^2 + \left(\frac{W(I,J+1,K) - (1/2)[W(I+1,J,K) + W(I-1,J,K)]}{\Delta Y_+}\right)^2\right]^{1/2}\Bigg\}$$
$$\cdot\left(\frac{U(I,J+1,K) - (1/2)[U(I+1,J,K) + U(I-1,J,K)]}{\Delta Y_+}\right) - \left\{1 + \left(\frac{L^2(J) + L^2(J-1)}{2}\right)\right.$$
$$\cdot\left[\left(\frac{(1/2)[U(I+1,J,K) + U(I-1,J,K)] - U(I,J-1,K)}{\Delta Y_-}\right)^2 + \left(\frac{(1/2)[W(I+1,J,K) + W(I-1,J,K)] - W(I,J-1,K)}{\Delta Y_-}\right)^2\right]^{1/2}\Bigg\}$$
$$\left.\cdot\left(\frac{(1/2)[U(I+1,J,K) + U(I-1,J,K)] - U(I,J-1,K)}{\Delta Y_-}\right)\right) \tag{24}$$

Z-momentum:

$$U(I,J,K)\left(\frac{W(I+1,J,K) - W(I-1,J,K)}{(\Delta X_+ + \Delta X_-)}\right) + V(I,J,K)\left(\frac{W(I,J+1,K) - W(I,J-1,K)}{(\Delta Y_+ + \Delta Y_-)}\right) + W(I,J,K)\left(\frac{W(I,J,K) - W(I,J,K-1)}{\Delta Z}\right) = UE(I,K)\left(\frac{WE(I+1,K) - WE(I-1,K)}{(\Delta X_+ + \Delta X_-)}\right) + WE(I,K)\left(\frac{WE(I,K) - WE(I,K-1)}{\Delta Z}\right) + \frac{2}{(\Delta Y_+ + \Delta Y_-)}\left(\left\{1 + \left(\frac{L^2(J+1) + L^2(J)}{2}\right)\right.\right.$$
$$\cdot\left[\left(\frac{U(I,J+1,K) - (1/2)[U(I+1,J,K) + U(I-1,J,K)]}{\Delta Y_+}\right)^2 + \left(\frac{W(I,J+1,K) - (1/2)[W(I+1,J,K) + W(I-1,J,K)]}{\Delta Y_+}\right)^2\right]^{1/2}\Bigg\}$$
$$\cdot\left(\frac{W(I,J+1,K) - (1/2)[W(I+1,J,K) + W(I-1,J,K)]}{\Delta Y_+}\right) - \left\{1 + \left(\frac{L^2(J) + L^2(J-1)}{2}\right)\right.$$
$$\cdot\left[\left(\frac{(1/2)[U(I+1,J,K) + U(I-1,J,K)] - U(I,J-1,K)}{\Delta Y_-}\right)^2 + \left(\frac{(1/2)[W(I+1,J,K) + W(I-1,J,K)] - W(I,J-1,K)}{\Delta Y_-}\right)^2\right]^{1/2}\Bigg\}$$
$$\left.\cdot\left(\frac{(1/2)[W(I+1,J,K) + W(I-1,J,K)] - W(I,J-1,K)}{\Delta Y_-}\right)\right) \tag{25}$$

Continuity:

$$\frac{U(I+1,J,K) + U(I+1,J-1,K) - U(I-1,J,K) - U(I-1,J-1,K)}{2(\Delta X_+ + \Delta X_-)} + \frac{V(I+1,J,K) - V(I+1,J-1,K)}{\Delta Y_-} + \frac{W(I+1,J,K) + W(I+1,J-1,K) - W(I+1,J,K-1) - W(I+1,J-1,K-1)}{2\Delta Z} = 0 \tag{26}$$

For a solution of properties at level $I + 1$, the Dufort-Frankel formulation requires knowledge at two earlier I levels, $I - 1$,

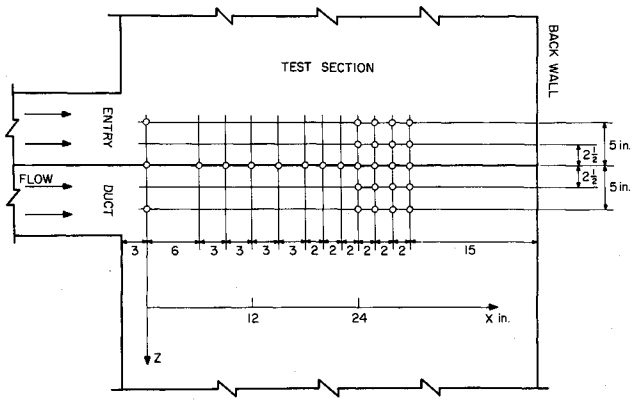

Fig. 3 Johnston geometry experimental data locations.

and I. This information was generated by a standard explicit formulation with the difference equations given below

X-momentum:

$$U(I,J,K)\left[\frac{U(I+1,J,K)-U(I,J,K)}{\Delta X_+}\right] + V(I,J,K)\left[\frac{U(I,J,K)-U(I,J-1,K)}{\Delta Y_-}\right]^* + W(I,J,K)\left[\frac{U(I,J,K)-U(I,J,K-1)}{\Delta Z}\right] = UE(I,K)\left[\frac{UE(I+1,K)-UE(I,K)}{\Delta X_+}\right] + WE(I,K)\left(\frac{UE(I,K)-UE(I,K-1)}{\Delta Z}\right) + \frac{2}{(\Delta Y_+ + \Delta Y_-)}\left(\left\{1+\left(\frac{L^2(J+1)+L^2(J)}{2}\right)\cdot\left[\left(\frac{U(I,J+1,K)-U(I,J,K)}{\Delta Y_+}\right)^2+\left(\frac{W(I,J+1,K)-W(I,J,K)}{\Delta Y_+}\right)^2\right]^{1/2}\right\}\cdot\left(\frac{U(I,J+1,K)-U(I,J,K)}{\Delta Y_+}\right)-\left\{1+\left(\frac{L^2(J)+L^2(J-1)}{2}\right)\cdot\left[\left(\frac{U(I,J,K)-U(I,J-1,K)}{\Delta Y_-}\right)^2+\left(\frac{W(I,J,K)-W(I,J-1,K)}{\Delta Y_-}\right)^2\right]^{1/2}\right\}\cdot\left(\frac{U(I,J,K)-U(I,J-1,K)}{\Delta Y_-}\right)\right) \quad (27)$$

Z-momentum:

$$U(I,J,K)\left(\frac{W(I+1,J,K)-W(I,J,K)}{\Delta X_+}\right) + V(I,J,K)\left(\frac{W(I,J,K)-W(I,J-1,K)}{\Delta Y_-}\right)^* + W(I,J,K)\left(\frac{W(I,J,K)-W(I,J,K-1)}{\Delta Z}\right) = UE(I,K)\left(\frac{WE(I+1,K)-WE(I,K)}{\Delta X_+}\right) + WE(I,K)\left(\frac{WE(I,K)-WE(I,K-1)}{\Delta Z}\right) + \frac{2}{(\Delta Y_+ + \Delta Y_-)}\left(\left\{1+\left(\frac{L^2(J+1)+L^2(J)}{2}\right)\cdot\left[\left(\frac{U(I,J+1,K)-U(I,J,K)}{\Delta Y_+}\right)^2+\left(\frac{W(I,J+1,K)-W(I,J,K)}{\Delta Y_+}\right)^2\right]^{1/2}\right\}\cdot\left(\frac{W(I,J+1,K)-W(I,J,K)}{\Delta Y_+}\right)-\left\{1+\left(\frac{L^2(J)+L^2(J-1)}{2}\right)\cdot\left[\left(\frac{U(I,J,K)-U(I,J-1,K)}{\Delta Y_-}\right)^2+\left(\frac{W(I,J,K)-W(I,J-1,K)}{\Delta Y_-}\right)^2\right]^{1/2}\right\}\cdot\left(\frac{W(I,J,K)-W(I,J-1,K)}{\Delta Y_-}\right)\right) \quad (28)$$

Continuity:

$$\frac{U(I+1,J,K)+U(I+1,J-1,K)-U(I,J,K)-U(I,J-1,K)}{2(\Delta X_+)} + \frac{V(I+1,J,K)-V(I+1,J-1,K)}{\Delta Y_-} + \frac{W(I+1,J,K)+W(I+1,J-1,K)-W(I+1,J,K-1)}{2\Delta Z} - \frac{W(I+1,J-1,K-1)}{2\Delta Z}=0 \quad (29)$$

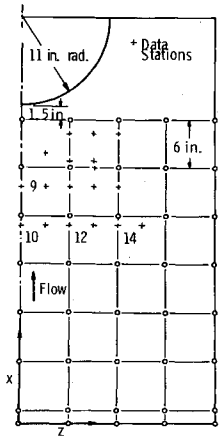

Fig. 4 Hornung and Joubert experimental stations.

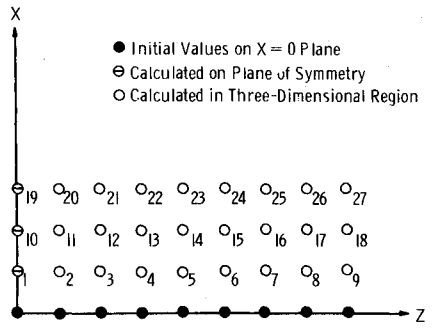

Fig. 5 Solution sequence on a Y plane.

The von Neumann stability criteria placed a severe x-step-size restriction on these equations and hence they were used for only about 30 steps before switching to the more efficient DuFort-Frankel formulation. In principle only one step needed to be taken with the standard explicit scheme but experience suggested a better transition between computing schemes occurred with the switch over delayed for a short distance.

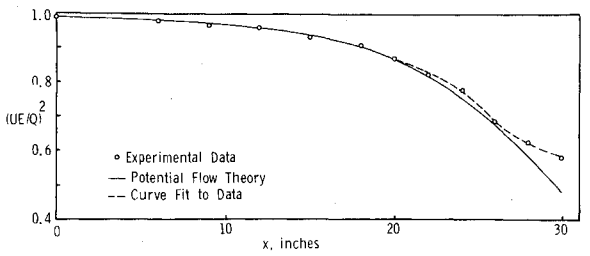

Fig. 6 Freestream boundary condition for the Johnston geometry on the plane of symmetry.

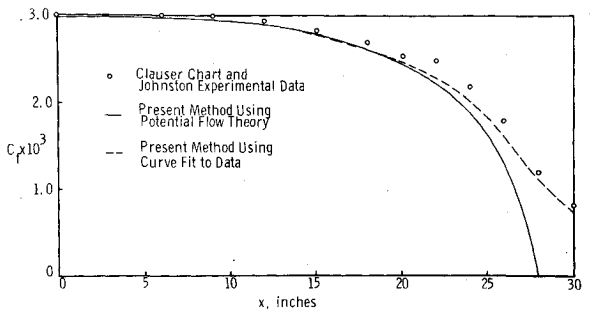

Fig. 7 Calculated and experimental values of local skin-friction coefficients on the plane of symmetry.

The necessary boundary condition for the z direction followed from solution to the plane of symmetry flow. As with the full three-dimensional flow standard explicit scheme was used to move out 30 steps, and simultaneous with the full solution the plane of symmetry solution was switched to the more efficient DuFort-Frankel formulation. The difference equations for the plane of symmetry are written from Eqs. (21–23) following the forms just given at the Z level of K-1.

All the difference equations are written for a variable grid spacing in X and Y. Asterisk-marked terms in Eqs. (27) and (28), and corresponding terms for the plane of symmetry, must be replaced by their forward difference counterparts if the normal velocity component becomes negative so that stability of the equation can be controlled by a change in the marching step size, ΔX_+. Pletcher[13] experienced this same problem and gives references to other workers who have had similar difficulties.

The basic differences in the DuFort-Frankel and explicit scheme may be seen by inspection of the x-momentum equation. The first derivative with respect to the X coordinate or marching direction is written as a forward difference in the simple explicit scheme and a central difference in the DuFort-Frankel scheme. The second derivation along the Y coordinate at the I, J node written in the Dufort-Frankel scheme uses an average of the variable value at the $I + 1$ and $I - 1$ plane nodes on the J plane, whereas the simple explicit scheme uses the variable value at the I node on the J plane.

The truncation error of the second derivative written in the DuFort-Frankel scheme contains a term of order $(\Delta X/\Delta Y)^2$ and although this term itself could be quite large in a given solution, the coefficient of this term is a second derivative with respect to the streamwise direction, which is known to be small in comparison to the derivatives with respect to the Y coordinate in any boundary-layer solution. For a more complete analysis of truncation errors and stability criterion pertaining to this method the reader is referred to the detailed solution by East,[16] and the summary for the two-dimensional case by Pletcher.[13]

Solution Geometries and Technique

The flow geometries chosen for solution were those investigated experimentally by Johnston[14] and Hornung and Joubert[17] and shown in Fig. 1. Figures 3 and 4 show the coordinate axes and stations where detailed comparisons of the analytical results with experimental data were made.

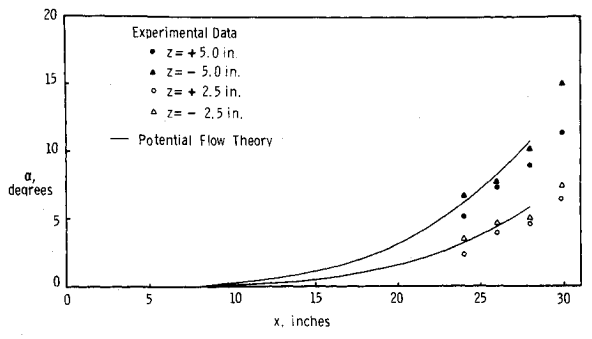

Fig. 8 Angle between the freestream velocity vector and the plane of symmetry for the Johnston geometry.

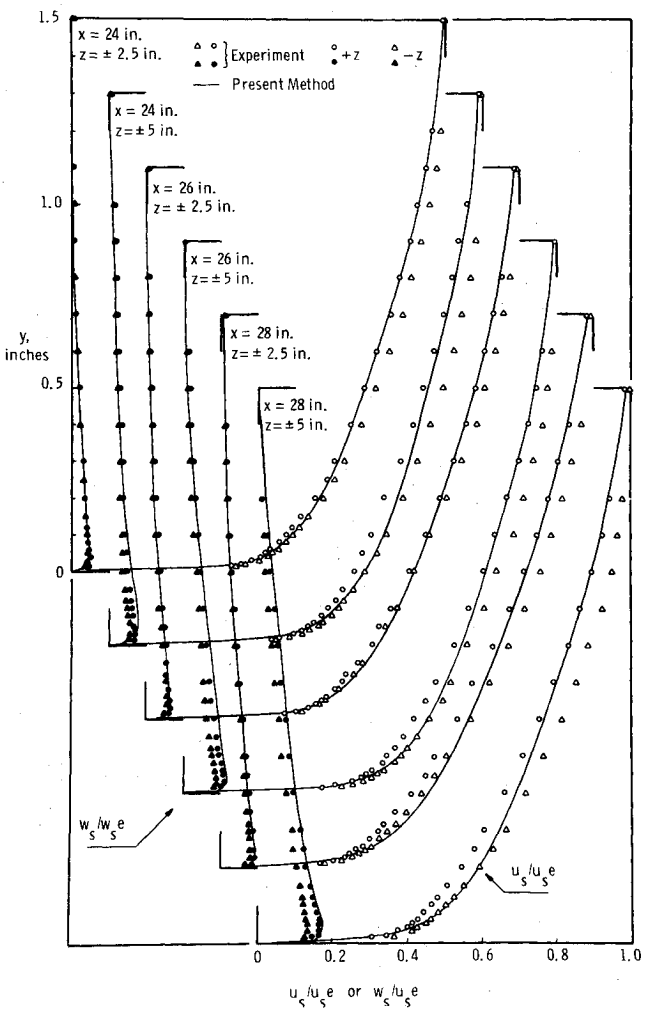

Fig. 9 Computed velocity profiles compared with the Johnston experimental data.

The external boundary conditions for the Johnston geometry was assumed to be that of two jets of fluid with velocity magnitudes, Q, originating at $\pm$ infinity on the x axis and impinging at the origin (location of the back wall). For a detailed derivation of the potential flow see Pai[18] and Milne-Thomson.[19] The external boundary conditions for the Hornung and Joubert geometry were taken to be those of an inviscid flow around a circular cylinder.

The boundary conditions required to start the solution at an X plane were taken from a two-dimensional solution started at the leading edge of a flat plate. This solution carried out and matched as closely as possible the first reported experimental data, after which the full three-dimensional flowfield solution was begun. Figure 5 shows the solution sequence of the finite-difference equations used for the three-dimensional geometries. At each Y plane location the variables were calculated by starting at the wall and proceeding outward through the boundary layer until the total velocity vector magnitude reached a value greater than 0.9995 of the freestream velocity vector magnitude. The Y plane node locations on the plane of symmetry used the plane of symmetry difference equations and those nodes in the three-dimensional region used the full three-dimensional difference equations. Once the solution had proceeded for about 30 marching steps along the X direction the simple explicit difference equations were replaced by the DuFort-Frankel formulation and the solution continued.

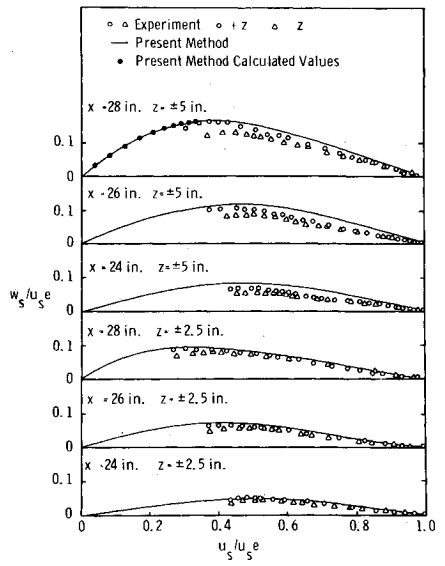

Fig. 10 Polar plots showing the Johnston experimental data and the present solution method.

Comparison of Results

Johnston Geometry

In a comparison of the calculated and experimental results for the Johnston[14] geometry note that the experimental freestream flowfield did not show good agreement with the potential flow solution near the back wall. This is ascribed to a buildup of displacement thickness on the closely spaced top and bottom boundary walls of the channel causing a slightly converging flow. A separate solution along the plane of symmetry using a sixth-order polynomial fitted to the experimental data for the freestream velocity UE, as shown in Fig. 6, leads to significantly better agreement with the experiment in the region of separation. The values of the skin-friction coefficient determined from Newton's law of friction closely approximated those values presented by Johnston and obtained by use of a Clauser chart; and values of displacement thickness, momentum thickness, and shape factor were also in excellent agreement with experiment. Fig. 7 shows that using the potential flow theory for the freestream boundary conditions resulted in an acceptable solution to an x value of 28 in. where the magnitude of the skin-friction coefficient, C_f, approached zero and the solution was stopped.

In the full three-dimensional flowfield solution, the edge conditions were taken from the potential flow solution since it was impractical to fit the relatively sparse experimental data. Figure 8 also emphasizes the unsymmetrical nature of the freestream streamline angle (angle between the freestream streamline and the plane of symmetry) of the Johnston experimental data. Also shown is the potential flow value of the freestream streamline angle. For x values less than 26 in. the potential flow solution predicts larger streamline angles than obtained in the experiment. The present computation compared with the experimental data emphasizes the unsymmetrical nature of the experimental flow, hence experimental data are presented for both sides of the plane of symmetry. Representative comparisons are made here, with extensive results and additional detailed comparisons available in East.[16]

Figure 9 shows the freestream and transverse components of the boundary-layer velocities for $x = 24$, 26, and 28 in. and $z = \pm 2.5$ and ± 5 in. The computer solution predicted separation on $z = 0$ at $x \approx 28$ in. and the program was terminated; and experimental data were not reported beyond $z = \pm 5$ in. These same profiles are shown in polar plots in Fig. 10. In general, velocity profiles on the plane of symmetry were in excellent agreement, and are not shown. The experimental results generally straddled the calculated freestream profiles, but transverse profiles were usually calculated in agreement with, or larger than measured. Polar plots for $z = \pm 2.5$ in. were also in closer and nearly perfect agreement with experiment as might be expected with lesser skewing, where transverse velocities were generally 10% or less than freestream velocities.

The skewed flow at $x = 28$ in. and $z = 5$ in., shown in a polar plot in Fig. 10, shows ten y-grid locations closer to the wall than were obtained experimentally. Particular interest centers on the near-wall region where the question of the existence of a collateral wall layer is raised. A number of investigators, Johnston,[14] Gardow,[20] Francis and Pierce,[21] Klinksiek and Pierce,[22] Hornung and Joubert,[17] M. Smith,[23] P.D. Smith,[24] Lewkowicz,[25] and Prahlad[26] all show from two up to seven experimentally determined points which suggest a collateral near-wall region of flow when w/U is plotted against u/U in a velocity polar. (Smith[24] also shows some profiles with an abrupt change in flow direction near the wall.) Rogers and Head,[27] using a more refined and miniature type probe for three-dimensional boundary layer measurements, have reported a single profile with strong skewing and with local flow angle varying continuously down to the wall. This instrument reports data at a total velocity ratio (local to freestream) of about 0.2 and this value generally occurs much closer to the wall than other experimenters have been able to probe.

For the shear model used in this analysis the present solution with several normal-grid locations well within the viscous sublayer showed no collateral or pseudo-two-dimensional region of flow near the wall. The first normal-grid location was at 0.001423 in., and the first presented experimental data were 0.014 in. from the wall. Figure 11 shows the lack of agreement between the computed and experimental streamline angles at a normal-coordinate location of 0.014 in. Also shown in the figure are the streamline angles calculated at a normal-coordinate location of 0.001423 in. In some cases the calculated local streamline angle nearly doubled its value as the normal-coordinate location moved from 0.014 in. to 0.001423 in. above the wall.

Figure 12 shows the local streamline angle with respect to the freestream streamline, plotted against the normal distance from the wall. These results clearly indicate a monotone increasing characteristic for the streamline angle approaching the wall. Figure 13 shows the near-wall details of Figure 12 and indicates a linear behavior of local flow angle near the wall. For this figure a solution was obtained where the first near-wall normal-grid location was at 0.000475 in. This linear behavior in the near-wall flow makes the inference of a limiting wall streamline angle, α_w, convenient. In all cases the inferred limiting wall streamline angles greatly exceeded the angles presented in the Johnston experimental data for the point nearest the wall. Within the viscous sublayer the mixing length is essentially zero and the usual boundary-layer equations are solved directly by the finite difference scheme. The fact that the solution in this region gives a (linear) variation of flow angle with wall distance infers that the assumption of a collateral near-wall flow region is not consistent with the motion equations themselves. Except for this point,

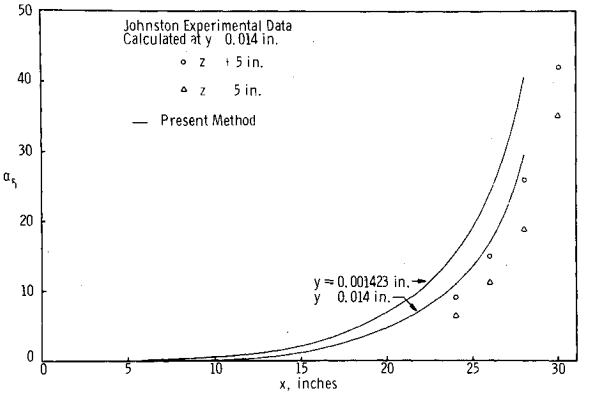

Fig. 11 Streamline angle at two y-coordinate locations for $z = 5$ in.

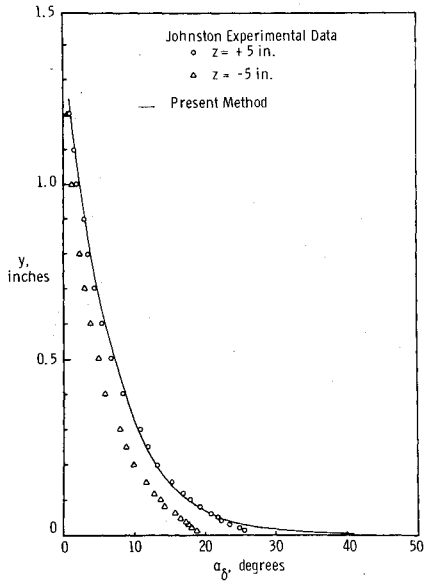

Fig. 12 Computed and experimental local flow angle with respect to the freestream direction; $x = 28$ in., $z = 5$ in.

the over-all agreement with the Johnston experimental data was considered as acceptable throughout the three-dimensional flowfield.

Hornung and Joubert Geometry

This numerical solution was obtained in much the same manner as the Johnston geometry solution. Since the Hornung and Joubert[17] geometry was not restricted on the top by a close bounding surface, as was the Johnston geometry, the displacement thickness buildup on the walls seemed to have little or no effect on the external boundary conditions; and the potential flow theory for flow around a circular cylinder agreed well with the experimental freestream velocity in front of the cylindrical obstruction.

A comparison of experimental and calculated streamwise velocity profiles at stations 12 and 14 is shown in Fig. 14. Polar plots of the calculated profiles and experimental data at these stations are shown in Fig. 15. Again, the present method of solution shows no collateral region near the wall.

Agreement of the present method of solution with the experimental data presented by Hornung and Joubert was excellent at stations 10, 12, and 14. No solution comparison at any other locations was made because the present solution technique was

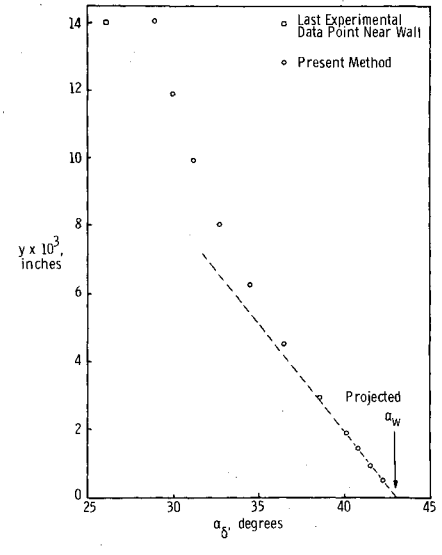

Fig. 13 Near-wall flow angle variation at $x = 28$ in., $z = 5$ in.

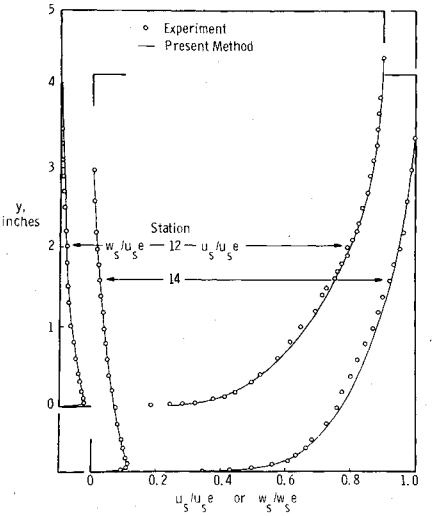

Fig. 14 Computed velocity profiles compared with Hornung and Joubert experimental data.

stopped just prior to reaching station 9 where C_f calculated from Newton's law of friction approached zero.

Three-Dimensional Solution Grid Spacing and Calculation Times

Because the Z-coordinate derivatives were not excessive, very large ΔZ-steps were taken without any adverse effects. For the Johnston geometry eight ΔZ-steps in 5 in. were used in the solution, and for the Hornung and Joubert geometry 16 ΔZ steps in 12 in. were used. Reducing the ΔZ step size by a factor of four showed no apparent effects on the solution. The solution on the plane of symmetry for the Johnston geometry required about 2 min on the IBM 360/65 digital computer. The three-dimensional solution for the Johnston geometry required about 1.25 hr, and the solution for the Hornung and Joubert geometry required nearly 2 hr. The large increase in computational time occurred because the three-dimensional DuFort-Frankel-type difference equations had to be linearized for a solution. No great effort has been placed on economizing the linearization technique to date.

Generally, for the three-dimensional solutions, the normal coordinate contained 80 grid points with closer spacing near the wall where large gradients occur. Doubling the number of grid locations across the boundary-layer thickness showed negligible effects. The first two or three normal-coordinate grid points were kept within the viscous sublayer where Newton's law of friction is valid. The shear stress inside the viscous sublayer was a constant, and as long as one normal-grid location was kept within the sublayer an acceptable value of shear stress was always obtained.

No general rule exists for specifying a maximum marching step size where convergence of the DuFort-Frankel difference equations, as used in this study, may be obtained. It was found by changing the marching step size that little or no effect on the boundary-layer parameters or profiles occurred when the mar-

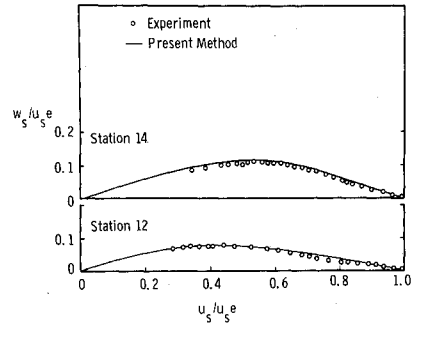

Fig. 15 Polar plots showing the Hornung and Joubert experimental data and the present solution method.

ching step size was less than 0.06 in. Approximately 450 marching steps were required to solve the three-dimensional geometries presented in this study.

The calculated results with comparison to experimental data indicate that the present solution method of the three-dimensional incompressible turbulent boundary-layer equations is adequate for predicting flows that have a plane of symmetry or for any geometry with known initial and boundary conditions.

Summary and Conclusions

A solution technique that uses a mixing-length theory mathematically model the turbulent shear stress terms has been extended to solve the three-dimensional turbulent flow problem, including plane of symmetry flows. The method of solution writes the governing boundary-layer equations in a generally stable explicit finite-difference form introduced initially by DuFort and Frankel[11] for the diffusion equation, and developed for two-dimensional turbulent boundary layers by Pletcher.[13]

Two similar three-dimensional flow geometries that were investigated experimentally by Johnston[14] and Hornung and Joubert[17] have been solved numerically. The solution technique is not limited to solving boundary-layer problems where a plane of symmetry exists but the boundary conditions required for a three-dimensional flowfiield are easily obtained when a plane of symmetry occurs in the flowfield. This is true since the flow on a plane of symmetry has only two independent variables and can be readily treated in the same manner as other two-dimensional fluid flow problems.

Prediction of the flow characteristics and parameters in a three-dimensional turbulent boundary-layer by the present method compared well with the available experimental data. The existence of a collateral region near the wall in a three-dimensional turbulent boundary-layer, as suggested by many experimentalists, was not seen in the solution. However the present experimental techniques, with exception given to the method of Rogers and Head,[27] probably cannot make accurate angle measurements close enough to the wall to prove or disprove the existence of a collateral region in the boundary-layer.

The results of this investigation strongly indicate that accurate three-dimensional predictions can be obtained by using a mixing, length theory to represent the turbulent shear stress terms in the momentum equations; however, only when more experimental turbulence data are taken under three-dimensional flow conditions can one determine the limitations that may exist on the Prandtl mixing-length hypothesis for three-dimensional flow conditions.

References

[1] Kline, S. J. et al, *Proceedings Computation of Turbulent Boundary Layers, 1968 AFOSR-IFP-Stanford Conference,* Vol. 1, *Methods, Predictions, Evaluation and Flow Structure,* Thermosciences Div., 1969, Stanford Univ., Stanford, Calif.

[2] *Compressible Turbulent Boundary Layers,* NASA SP-216, Dec. 1968.

[3] Crank, J. and P. Nicholson, "A Practical Method for Numerical Evaluation of Solutions of Partial Differential Equations of the Heat Conduction Types," *Proceedings of the Cambridge Philosophical Society,* Vol. 43, 1947, pp. 50–67; also *Applied Mechanics Review,* Vol. 1, 1948.

[4] Bradshaw, P., "Calculation of Boundary-Layer Development Using the Turbulent Energy Equation. VII. Three-Dimensional Flow," NPL Aero Rept. 1286, 1969, Aerodynamics Div., Her Majesty's Stationery Office, London.

[5] Nash, J. F., "The Calculation of Three-Dimensional Turbulent Boundary Layers in Incompressible Flow," *Journal of Fluid Mechanics,* Vol. 37, Pt. 4, 1969, pp. 625–642.

[6] Nash, J. F., "An Explicit Scheme for the Calculation of Three-Dimensional Turbulent Boundary Layers," *Transactions of the ASME: Journal of Basic Engineering,* Vol. 94, No. 1, 1972, pp. 131–141.

[7] Mellor, G. L., "Incompressible Turbulent Boundary Layers with Arbitrary Pressure Gradients and Divergent or Convergent Cross Flows," *AIAA Journal,* Vol. 5, No. 9, Sept. 1967, pp. 1570–1579.

[8] Hunt, J. L., D. Bushwell and I. Beckwith, "Finite Difference Analysis of the Compressible Turbulent Boundary Layer on a Blunt Swept Slab With Leading-Edge Blowing," *Analytical Methods in Aircraft Aerodynamics,* NASA SP-228, 1969, pp. 417–472.

[9] Maise, G. and H. McDonald, "Mixing Length and Kinematic Eddy Viscosity in a Compressible Boundary Layer," *AIAA Journal,* Vol. 6, No. 1, Jan. 1968, pp. 73–80.

[10] van Driest, E. R., "On Turbulent Flow Near a Wall," *Journal of the Aeronautical Sciences,* Vol. 23, 1956, pp. 1007–1011.

[11] DuFort, E. C. and S. P. Frankel, "Stability Conditions in the Numerical Treatment of Parabolic Differential Equations," *Mathematical Tables and Other Aids to Computation,* Vol. 7, 1953, p. 135.

[12] Goldstein, S., *Modern Developments in Fluid Dynamics,* Vol. 1, Dover, New York, 1965, pp. 205–210.

[13] Pletcher, R. H., "On a Finite Difference Solution for the Constant Property Turbulent Boundary Layer," *AIAA Journal,* Vol. 7, No. 2, Feb. 1969, pp. 305–311.

[14] Johnston, J. P., "Three-Dimensional Turbulent Boundary Layer," Rept. 39, 1957, MIT Gas Turbine Lab., Cambridge, Mass.; also "On the Three-Dimensional Turbulent Boundary Layer Generated by Secondary Flow," and "Turbulent Boundary Layer at the Plane of Symmetry in a Three-Dimensional Flow," *Transactions of the ASME: Journal of Basic Engineering,* Vol. 82, No. 3, 1960, pp. 233–246, pp. 622–628.

[15] O'Brien, G. G., M. A. Hyman, and S. Kaplan, "A Study of the Numerical Solution of Partial Differential Equations," *Journal of Mathematics and Physics,* Vol. 29, No. 4, 1951, pp. 223–241.

[16] East, J. L., Jr., "An Exact Numerical Solution of the Three-Dimensional Incompressible Turbulent Boundary-Layer Equations," Ph. D. dissertation, 1970, Virginia Polytechnic Inst. and State Univ.

[17] Hornung, H. G. and P. N. Joubert, "The Mean Velocity Profile in Three-Dimensional Turbulent Boundary Layers," *Journal of Fluid Mechanics,* Vol. 15, Pt. 3, 1962, pp. 368–384.

[18] Pai, S. I., *Fluid Dynamics of Jets,* D. Van Nostrand, New York, 1954, pp. 9–13.

[19] Milne-Thomson, L. M., *Theoretical Hydrodynamics,* Macmillan, New York, 1955, pp. 283–289.

[20] Gardow, E., "The Three-Dimensional Turbulent Boundary Layer in a Free Vortex Diffuser," Rept. 42, 1958, MIT Gas Turbine Lab., Cambridge, Mass.

[21] Francis, G. P. and F. J. Pierce, "An Experimental Study of Skewed Turbulent Boundary Layers in Low Speed Flows," *Transactions of the ASME, Ser. D: Journal of Basic Engineering,* Vol. 89, 1967, pp. 597–608.

[22] Klinksiek, W. F. and F. J. Pierce, "Simultaneous Lateral Skewing in a Three-Dimensional Turbulent Boundary Layer Flow," *Transactions of the ASME, Ser. D: Journal of Basic Engineering,* Vol. 92, 1970, pp. 83–92.

[23] Smith, M., "Incompressible Skewed Turbulent Boundary Layer on an End Wall of a Curved Two-Dimensional Diffser," Doctoral dissertation, 1970, Iowa State Univ. of Science and Technology, Ames, Iowa.

[24] Smith, P. D., "Calculation Methods for Three-Dimensional Turbulent Boundary Layers," RM-3523, 1968, Aeronautical Research Council, Queens Univ., Belfast; also "An Investigation Into Three-Dimensional Boundary Layers," Doctoral dissertation, 1965, Univ. of London, England.

[25] Lewkowicz, A., "Two and Three-Dimensional Incompressible Turbulent Boundary Layers," Doctoral dissertation, 1965, Univ. of Liverpool, England.

[26] Prahlad, T. S., "Wall Similarity in Three-Dimensional Turbulent Boundary Layers," *AIAA Journal,* Vol. 6, No. 9, Sept. 1968, pp. 1772–1774; also private communication, 1969, now at National Aeronautical Lab., Bangalore, India.

[27] Rogers, B. K., and M. R. Head, "Measurement of Three-Dimensional Boundary Layers," *The Aeronautical Journal of the Royal Aeronautical Society,* Vol. 73, 1969, pp. 796–798.